Electronic Supplementary Material (ESI) for Journal of Materials Chemistry C.
This journal is © The Royal Society of Chemistry 2022

Supplemental Materials

Remote two-dimensional nanometric localization of molecules by the analysis of fluorescence coupled to guided surface plasmons

Pingzhun Ma,[a,b] Qiyong Tao,[a,b] Zhe Qi,[a,b] Yuhang Su,[a,b] Ying Zhong[c] and Haitao Liu*[a,b]

[a] Institute of Modern Optics, College of Electronic Information and Optical Engineering, Nankai University, Tianjin, 300350, China
[b] Tianjin Key Laboratory of Micro-scale Optical Information Science and Technology, Tianjin, 300350, China
[c] State Key Laboratory of Precision Measurement Technology and Instruments, Tianjin University, Tianjin 300072, China
*Corresponding author: liuht@nankai.edu.cn

CONTENT

S1. Preparation of the test sample and the reference sample

A. Preparation of the test sample

The surface of a coverslip is modified for 30s by the plasma cleaning, and then the aqueous solution of silver nanowires (NWs) is dripped onto the surface of the coverslip. Stand the sample in the air for 3~5min, rinse it with pure water for several times and blow it dry with N_2 gas. Thus the silver NWs are adsorbed on the glass substrate. Modify the sample by plasma cleaning again for 10~15s, making the glass surface and silver NWs negatively charged. Then the aqueous solution of Poly (diallyldimethylammonium chloride) (PDDA) is dripped onto the sample surface. Stand the sample in the air for 10min, rinse it with pure water for several times and blow it dry with N_2 gas. Thus the first layer of cationic polyelectrolyte (PE) is adsorbed on the surface. Then the aqueous solution of poly (sodium 4-styrenesulfonate) (PSS) is dripped onto the sample surface. Stand the sample in the air for

10min, rinse it with pure water for several times and dry it with N_2 gas. Then the first layer of anionic PE is adsorbed on the surface. Repeat the two steps of adsorption of cationic and anionic PE layers, so as to complete the adsorption of the multilayer PE with a specific thickness, with the outermost layer being PDDA. Next, polymethyl methacrylate (PMMA) is spin coated on the surface with a thickness of h=60nm (as shown in Fig. S3). This layer is called PMMA-1 which covers the whole glass surface and the bottom part of silver NWs, as shown by the white dashed line in Fig. 1(b) of the main text. The sample is then put on a hot plate at 160℃ for 20min in the air to enhance the adhesion between the PMMA-1 layer and the coverslip, so as to prevent the PMMA-1 layer from being damaged by the water solution in the next step. After the sample is naturally cooled to room temperature in the air, the aqueous solution of fluorescent molecule A647 (1μmol/L) is dripped onto the sample surface. Stand the sample in the air for 5~10min, then rinse it with pure water for several times and blow it dry with N_2 gas. In this way, the negatively charged A647 molecules in aqueous solution are only adsorbed onto the outmost PDDA layer that wraps the silver NW and on the NW's top part [h=60 nm as sketched in Fig. 1(b)] which is determined by the PMMA-1 layer, and the fluorescent molecules at other positions on the surface of PMMA-1 layer are washed away. Finally, another layer of PMMA (this layer is called PMMA-2) with a thickness of about 350nm is spin coated on the surface.

B. Preparation of the reference sample

A PE layer with a thickness of d=19nm is adsorbed on the surface of a clean coverslip. The aqueous solution of fluorescent molecules A647 (1μmol/L) is dripped onto the sample surface. Stand the sample in the air for 5~10min, rinse it with pure water for several times and blow it dry with N_2 gas. In this way, A647 molecules are uniformly adsorbed on the whole sample surface. Finally, a layer of PMMA with a thickness of about 350nm is spin coated on the surface. The measurements for the reference sample are carried out with the same oil immersion objective (100×, NA=1.49) as sketched in Fig. 1(a) of the main text (without the silver NWs).

S2. Additional experimental and theoretical details for the remote radial localization of molecules

A. Preparation and measurement of the PE layer and PMMA-1 layer

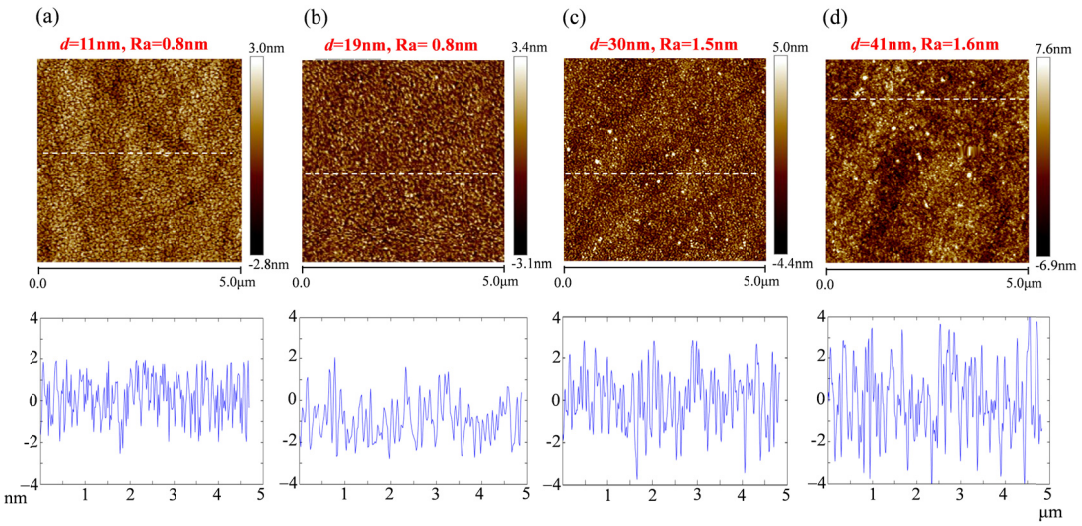

Fig. S1 Surface topography of the PE layer measured by AFM, with the thickness of PE layer being 11 nm (a), 19 nm (b), 30 nm (c), 41 nm (d), respectively. The upper images show that the surface roughnesses Ra of the PE layer are about 0.8, 0.8, 1.5, 1.6 nm, respectively. The lower figures show the height distribution along the white dashed lines in the upper images.

In the experiment, we used two PDDA solutions (called PDDA1 and PDDA2) and two PSS solutions (called PSS1 and PSS2). PDDA1 is an aqueous solution of PDDA (concentration 1v/v%, i.e., the volume of PDDA accounts for 1% of the volume of the aqueous solution), and PDDA2 is a mixed aqueous solution of PDDA and NaCl (PDDA: 1v/v%, NaCl: 0.25 mol/L). PSS1 is an aqueous solution

of PSS (50v/v%), and PSS2 is a mixed aqueous solution of PSS and NaCl (PSS: 50v/v%, NaCl: 0.25 mol/L). The adsorption procedure for each layer of PE is the same as described in Section S1A. The PE layer with different thicknesses d were prepared as follows.

d=11 nm: PDDA2→PSS2→PDDA1→PSS1→PDDA1.

d=19 nm: PDDA2→PSS2→PDDA2→PSS2→PDDA2→PSS2→PDDA1.

d=30 nm: PDDA2→PSS2→PDDA2→PSS2→PDDA2→PSS2→PDDA2→PSS2→PDDA1.

d=41 nm: PDDA2→PSS2→PDDA2→PSS2→PDDA2→PSS2→PDDA2→PSS2→PDDA2 →PSS2→PDDA1.

For these four samples with different values of d, the surface topography of the PE layer adsorbed on the surface of a glass coverslip was measured by atomic force microscope (AFM), as shown in Fig. S1, and the thickness of the PE layer was measured by an AFM scratch test, as shown in Fig. S2.

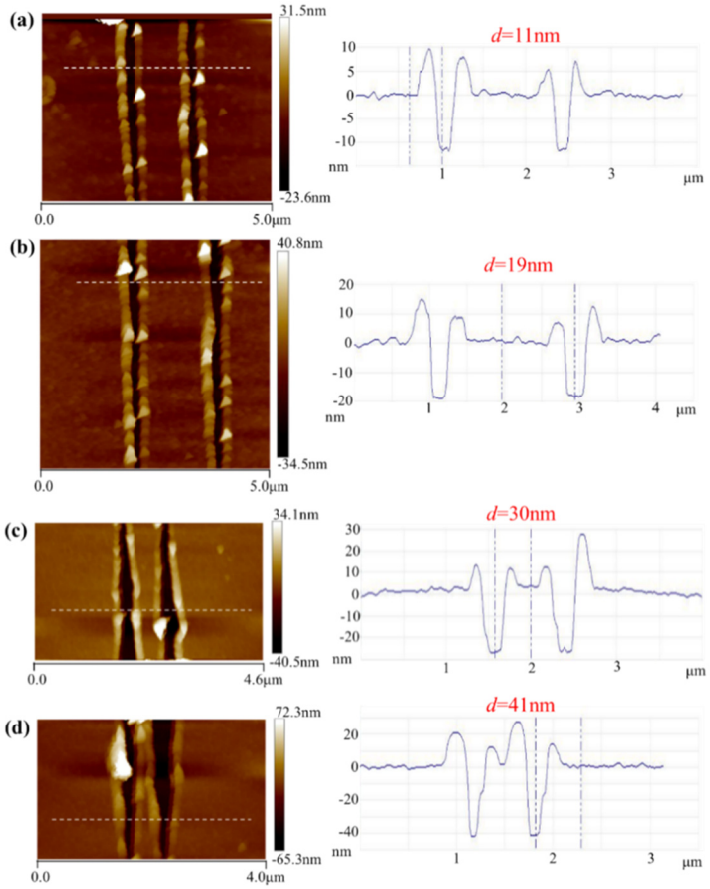

Fig. S2 Measurement of the thicknesses of the PE layers. The measured thicknesses are d=11 nm (**a**), 19 nm (**b**), 30 nm (**c**) and 41 nm (**d**). In (a)-(d), the trenches in the AFM images (left column) are scratched by the AFM probe. The figures in the right column show the height distributions along the white dashed lines in the AFM images. The height difference between the locations of the two vertical dash-dotted lines determines the value of d.

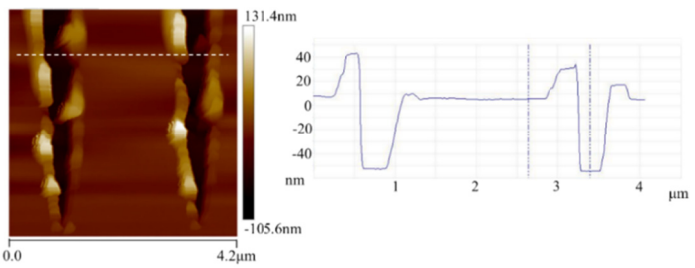

Fig. S3 Measurement of the thickness of PMMA-1 layer. The PMMA is spin coated on the surface of a coverslip, without the PE layer underneath. The trench in the AFM image (left figure) is scratched by the AFM probe. The right figure shows the height distribution along the white dashed line in the AFM image. The height difference between the locations of the two vertical dash-dotted lines determines the thickness of PMMA-1, which is about 60nm.

B. Additional SEM imaging of the silver nanowire without and with the adsorption of PE layer

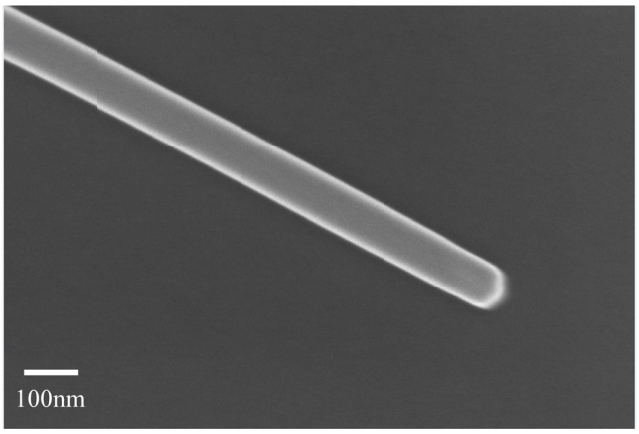

Fig. S4 SEM imaging of a bare silver nanowire (on silicon substrate) without the adsorption of PE layer.

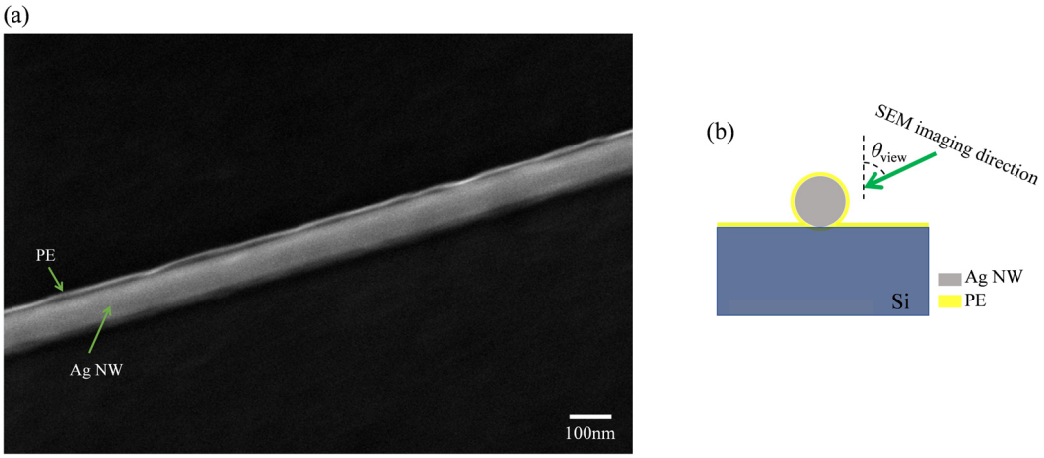

Fig. S5 SEM imaging of a silver nanowire (on silicon substrate) with the adsorption of PE layer (thickness 19 nm) (a), which is taken from a side view (θ_{view}>60°) as illustrated in (b).

C. Definition and calculation of the Γ_{SPP}, Γ_{rad} and Γ_{loss}

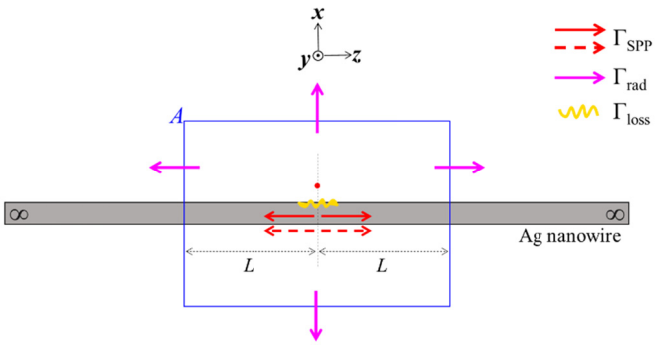

Fig. S6 Schematic diagram of the three emission channels (Γ_{SPP}, Γ_{rad}, Γ_{loss}) of an emitter (red dot) coupled with a silver nanowire of infinite length. Channel 1 (red solid and dashed arrows) is the coupling to the bounded and propagative fundamental SPP modes on the NW, with a coupling rate Γ_{SPP}. Channel 2 (purple arrows) is the emission into the homogeneous surrounding medium around the NW, with a far-field emission rate Γ_{rad}. Channel 3 (yellow wavy line) is the ohmic loss induced by the metal near the point source, with a loss rate Γ_{loss}.

In the coupling system of an excited fluorescent molecule and an infinite-length silver NW as shown in Fig. 3(a) of the main text, the molecule is represented by a point source, expressed as an electric-current density $\mathbf{J}=\delta(\mathbf{r}-\mathbf{r}_0)\mathbf{p}$. The schematic diagram of the emission channels of the point

source is shown in Fig. S6. The physical meanings of the three emission channels have been discussed in Section 3.2A of the main text. In Fig. S6, the blue rectangle represents a closed surface A ($2L$ in length, near the point source), which contains the point source and part of the silver NW. The emission of the point source satisfies the energy conservation law of the electromagnetic field,

$$-\frac{1}{2}\mathrm{Re}\left[\mathbf{E}^*_{\mathrm{total}}(\mathbf{r}_0)\cdot\mathbf{p}\right]=\oiint_A\frac{1}{2}\mathrm{Re}(\mathbf{E}_{\mathrm{total}}\times\mathbf{H}^*_{\mathrm{total}})\cdot\mathbf{n}da+\iiint_V\frac{1}{2}\omega\varepsilon''|\mathbf{E}_{\mathrm{total}}|^2dv\,, \tag{S1}$$

where $\mathbf{E}_{\mathrm{total}}$ and $\mathbf{H}_{\mathrm{total}}$ are the electric and magnetic field vectors excited by the point source, respectively, $\mathbf{n}$ is the outward normal unit vector on surface A, V is the region enclosed by A, ε'' is the imaginary part of the permittivity of the materials in region V, $\omega=k_0c$ is the angular frequency, and c is the speed of light in the vacuum. The term on the left side of Eq. (S1) represents the total emission power (i.e., the total spontaneous emission rate, denoted by Γ_{T}) of the point source, and the first and second terms on the right side represent the energy flux out of A and the ohmic loss in V, respectively.

The first term on the right side of Eq. (S1) consists of two parts: one part is the emission into the surrounding homogeneous medium (that is, the far-field emission rate, denoted by Γ_{rad}, shown by the purple arrows in Fig. S6), and the other part is the coupling to the two bounded and propagative SPP modes on the silver NW [see Fig. 3(c), (d1)-(d2) in the main text], that is,

$$\oiint_A\frac{1}{2}\mathrm{Re}(\mathbf{E}_{\mathrm{total}}\times\mathbf{H}^*_{\mathrm{total}})\cdot\mathbf{n}da=\Gamma_{\mathrm{rad}}+|\exp(ik_0n^1_{\mathrm{eff}}L)|^2\,\Gamma_{\mathrm{SPP1}}+|\exp(ik_0n^2_{\mathrm{eff}}L)|^2\,\Gamma_{\mathrm{SPP2}}\,, \tag{S2}$$

where the factor $|\exp(ik_0n^i_{\mathrm{eff}}L)|^2$ (i=1, 2) originates from the propagation loss experienced by the SPP mode i that propagates from the position of the point source to surface A. The definitions and calculation methods of n^i_{eff} and $\Gamma_{\mathrm{SPP}i}$ (i=1, 2) are given in Section 3.2B of the main text. From Eq. (S2), we can obtain the definition of Γ_{rad} as,

$$\Gamma_{\mathrm{rad}}=\oiint_A\frac{1}{2}\mathrm{Re}(\mathbf{E}_{\mathrm{total}}\times\mathbf{H}^*_{\mathrm{total}})\cdot\mathbf{n}da-|\exp(ik_0n^1_{\mathrm{eff}}L)|^2\,\Gamma_{\mathrm{SPP1}}-|\exp(ik_0n^2_{\mathrm{eff}}L)|^2\,\Gamma_{\mathrm{SPP2}}\,. \tag{S3}$$

The second term on the right side of Eq. (S1) represents the ohmic loss introduced by the metal inside the closed surface A, which consists of two parts: one part is the ohmic loss induced by the metal adjacent to the point source (that is, the loss rate, denoted by Γ_{loss}, shown by the yellow wavy line in Fig. S6), and the other part is the propagation loss of the two fundamental bounded and propagative SPP modes that propagate over a distance L, that is,

$$\begin{aligned}\iiint_V\frac{1}{2}\omega\varepsilon''|\mathbf{E}_{\mathrm{total}}|^2dv&=\Gamma_{\mathrm{loss}}+[1-|\exp(ik_0n^1_{\mathrm{eff}}L)|^2]\Gamma_{\mathrm{SPP1}}+[1-|\exp(ik_0n^2_{\mathrm{eff}}L)|^2]\Gamma_{\mathrm{SPP2}}\\&=\Gamma_{\mathrm{loss}}+[\Gamma_{\mathrm{SPP}}-|\exp(ik_0n^1_{\mathrm{eff}}L)|^2\Gamma_{\mathrm{SPP1}}-|\exp(ik_0n^2_{\mathrm{eff}}L)|^2\,\Gamma_{\mathrm{SPP2}}],\end{aligned} \tag{S4}$$

with $\Gamma_{\mathrm{SPP}}=\Gamma_{\mathrm{SPP1}}+\Gamma_{\mathrm{SPP2}}$ [see this before Eq. (2) in the main text]. Γ_{SPP} is the coupling rate/power of the two bounded and propagative SPP modes on the cross-section where the point source is located, as indicated by the red solid and dashed arrows in Fig. S6. From Eq. (S4), we can obtain the definition of Γ_{loss} as

$$\Gamma_{\mathrm{loss}}=\iiint_V\frac{1}{2}\omega\varepsilon''|\mathbf{E}_{\mathrm{total}}|^2dv-[\Gamma_{\mathrm{SPP}}-|\exp(ik_0n^1_{\mathrm{eff}}L)|^2\,\Gamma_{\mathrm{SPP1}}-|\exp(ik_0n^2_{\mathrm{eff}}L)|^2\,\Gamma_{\mathrm{SPP2}}]\,. \tag{S5}$$

Equation (S5) shows that Γ_{loss} does not contain the propagation loss of SPPs on the NW [that is, the terms in the square bracket on the right side of Eq. (S5)], which depends on the propagation distance L and is instead included in Γ_{SPP}. Substituting Eqs. (S2) and (S4) into the right side of Eq. (S1), it can be proved that Γ_{T}, Γ_{rad}, Γ_{SPP} and Γ_{loss} satisfy an energy-conservation relation,

$$\Gamma_{\mathrm{T}}=\Gamma_{\mathrm{rad}}+\Gamma_{\mathrm{SPP}}+\Gamma_{\mathrm{loss}}. \tag{S6}$$

The dependence of Γ_{SPP} on the distance d from the point source to the surface of the NW is shown in Fig. S7(a), which indicates that Γ_{SPP} of the radially polarized point source is significantly higher than that of the axially and azimuthally polarized point sources. Figure S7(b) shows the coupling rates Γ_{SPP1} (solid curve) and Γ_{SPP2} (dashed curve) of SPP modes 1 and 2 ($\Gamma_{\mathrm{SPP}}=\Gamma_{\mathrm{SPP1}}+\Gamma_{\mathrm{SPP2}}$) for the radially polarized point source, which are plotted as functions of d. For the point sources with different polarization directions, the dependences of Γ_{rad} and Γ_{loss} on d are shown in Fig. S7(c)-(d).

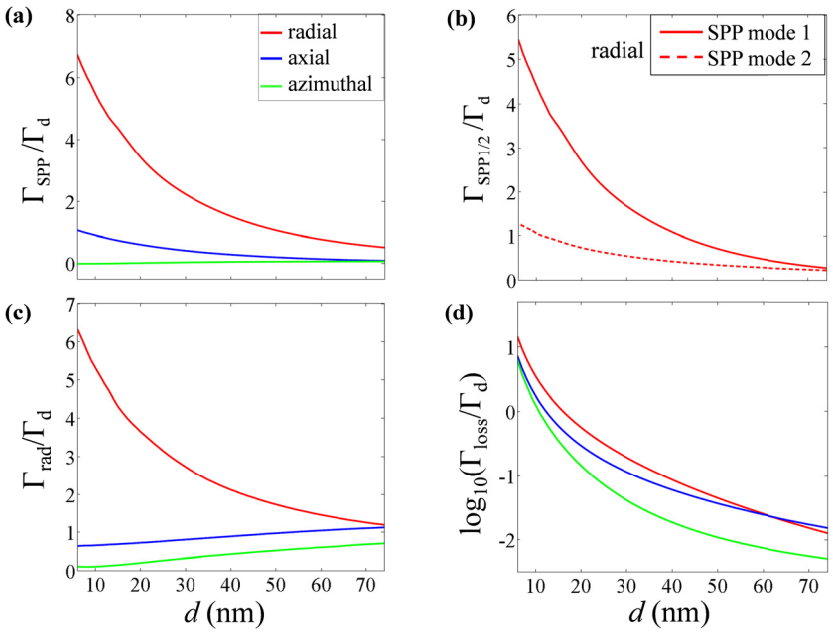

Fig. S7 Coupling rate Γ_{SPP} of SPP (a), coupling rate $\Gamma_{SPP1/2}$ of SPP mode 1 and mode 2 for the radially polarized point source (b), radiative emission rate Γ_{rad} (c), and loss rate Γ_{loss} (d), which are normalized by Γ_d and plotted as functions of the distance d from the point source to the surface of the silver NW. In (a), (c) and (d), the red, blue and green curves correspond to the radially, axially and azimuthally polarized point sources, respectively. The red solid and dashed curves in (b) correspond to SPP mode 1 and mode 2, respectively. The structural parameters can be found in Fig. 3 in the main text. The results in (a)-(b) are obtained with the full-wave aperiodic Fourier modal method (a-FMM),[1-3] and those in (c)-(d) are obtained with the full-wave finite element method (FEM).

D. Measurement of the intrinsic quantum yield η_d of A647 molecules in the reference sample and derivation of Eq. (1) in the main text for the fluorescence lifetime τ

At room temperature, the intrinsic quantum yield of A647 molecules in water (refractive index n_w=1.33) is $\eta_w=\Gamma_w/(\Gamma_w+\Gamma_{Aw})$=33% (provided by Invitrogen, and close to the value in the literature[4]), where Γ_w is the total spontaneous emission rate and Γ_{Aw} is the intrinsic loss rate of A647 molecules in water. Similarly, in the reference sample (corresponding to a homogeneous medium with a refractive index n_d=1.5), the intrinsic quantum yield of A647 molecules is expressed as $\eta_d=\Gamma_d/(\Gamma_d+\Gamma_{Ad})$, where Γ_d is the total spontaneous emission rate and Γ_{Ad} is the intrinsic loss rate of A647 molecules in the reference sample. In the following, we present the measurement of η_d.

First, the fluorescence lifetimes of A647 molecules in water and the reference sample were measured and are denoted by τ_w and τ_d, respectively. As shown in Fig. S8, there is $\tau_w=1/(\Gamma_w+\Gamma_{Aw})$=1.15 ns and $\tau_d=1/(\Gamma_d+\Gamma_{Ad})$=1.75 ns, where $\Gamma_w=\eta_{vac}k_0^2n_w/(12\pi)$ and $\Gamma_d=\eta_{vac}k_0^2n_d/(12\pi)$. Then there is,

$$\frac{\tau_w}{\tau_d}=\frac{\Gamma_d+\Gamma_{Ad}}{\Gamma_w+\Gamma_{Aw}}=\frac{\eta_w}{\eta_d}\cdot\frac{\Gamma_d}{\Gamma_w}, \tag{S7}$$

where $\Gamma_d/\Gamma_w=n_d/n_w$=1.5/1.33. Using Eq. (S7) and the values of τ_w, τ_d, η_w and Γ_d/Γ_w, we obtain η_d=57%.

After obtaining η_d, we can give the expression for the fluorescence lifetime τ of A647 molecules coupled with the silver NW in the test samples. The total decay rate of an excited molecule can be expressed as $\Gamma_\tau=\Gamma_T+\Gamma_{Ad}$, where Γ_T is the spontaneous emission rate (see Section 3.2A in the main text) and Γ_{Ad} is the intrinsic loss rate of the molecules in the test samples. Then according to

$$\frac{\tau}{\tau_d}=\frac{\Gamma_d+\Gamma_{Ad}}{\Gamma_T+\Gamma_{Ad}}=\frac{(\Gamma_d+\Gamma_{Ad})/\Gamma_d}{(\Gamma_T+\Gamma_{Ad})/\Gamma_d}=\frac{1/\eta_d}{\Gamma_T/\Gamma_d+(1/\eta_d-1)}=\frac{1}{\eta_d\Gamma_T/\Gamma_d+(1-\eta_d)}, \tag{S8}$$

τ can be expressed as

$$\tau=\frac{\tau_d}{\eta_d\Gamma_T/\Gamma_d+(1-\eta_d)}. \tag{S9}$$

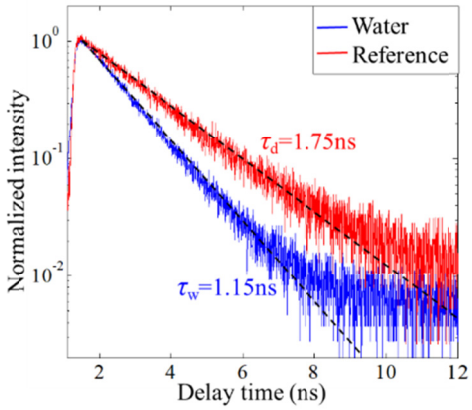

Fig. S8 Fluorescence decay curves of A647 molecules in water (blue curve) and the reference sample (red curve), with fluorescence lifetimes τ_w=1.15ns and τ_d=1.75ns, respectively. The black dashed lines are the fitted single-exponential function $A\exp(-t/\tau)$, where A is a constant, t is the delay time of the fluorescence emission, and τ is the fluorescence lifetime.

E. Total spontaneous emission rate Γ_T of a point source with an arbitrary polarization direction coupled with a silver nanowire

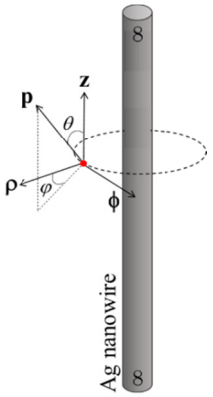

Fig. S9 Sketch of the coupling system composed of a fluorescent molecule (shown by the red dot) and a silver NW of infinite length. The molecule is represented by a point electric-current source with an arbitrary linear-polarization direction **p**.

The coupling system composed of a point electric-current source (representing the excited fluorescent molecule) and an infinite-length silver NW is shown in Fig. S9. In the following, we consider a point source with an arbitrary linear-polarization direction, which can be expressed as $\mathbf{J}=\delta(\mathbf{r}-\mathbf{r}_0)\mathbf{p}$, where $\mathbf{p}$ is a real-valued unit vector along the polarization direction, and $\mathbf{r}_0$ is the position of the point source. $\mathbf{p}$ can be expressed as $\mathbf{p}=\boldsymbol{\rho}\sin\theta\cos\varphi+\boldsymbol{\phi}\sin\theta\sin\varphi+\mathbf{z}\cos\theta=p_\rho\boldsymbol{\rho}+p_\phi\boldsymbol{\phi}+p_z\mathbf{z}$, with ($\boldsymbol{\rho}$, $\boldsymbol{\phi}$, $\mathbf{z}$) being the unit vectors along the radial, azimuthal, and axial directions of the NW. The definitions of θ and φ are illustrated in Fig. S9. The total spontaneous emission rate of the point source is expressed as

$$\Gamma_T^{(\mathbf{p})} = -\mathrm{Re}[\mathbf{E}^{(\mathbf{p})}(\mathbf{r}_0)\cdot\mathbf{p}]/2, \tag{S10}$$

where $\mathbf{E}^{(\mathbf{p})}(\mathbf{r}_0)$ is the electric-field vector at position $\mathbf{r}_0$ excited by the point source $\mathbf{J}$, and the superscript represents the polarization direction of the point source. In particular, for the radially, azimuthally and axially polarized point sources ($\mathbf{p}=\boldsymbol{\rho}$, $\boldsymbol{\phi}$, $\mathbf{z}$), the excited electric-field vectors are denoted by $\mathbf{E}^{(\boldsymbol{\rho})}$, $\mathbf{E}^{(\boldsymbol{\phi})}$ and $\mathbf{E}^{(\mathbf{z})}$, and the total spontaneous emission rates are $\Gamma_T^{(\boldsymbol{\rho})}=-\mathrm{Re}[E_\rho^{(\boldsymbol{\rho})}(\mathbf{r}_0)]/2$, $\Gamma_T^{(\boldsymbol{\phi})}=-\mathrm{Re}[E_\phi^{(\boldsymbol{\phi})}(\mathbf{r}_0)]/2$, and $\Gamma_T^{(\mathbf{z})}=-\mathrm{Re}[E_z^{(\mathbf{z})}(\mathbf{r}_0)]/2$, respectively, with the subscripts ρ, ϕ and z denoting the ρ-, ϕ- and z-components of the electric field, respectively.

According to the linear-superposition principle of the electromagnetic field, $\mathbf{E}^{(\mathbf{p})}$ can be expressed as

$$\mathbf{E}^{(\mathbf{p})}=p_\rho\mathbf{E}^{(\boldsymbol{\rho})}+p_\phi\mathbf{E}^{(\boldsymbol{\phi})}+p_z\mathbf{E}^{(\mathbf{z})}. \tag{S11}$$

Substituting Eq. (S11) into Eq. (S10), one can obtain

$$\begin{aligned}\Gamma_{\mathrm{T}}^{(\mathbf{p})} &= -\frac{1}{2}\mathrm{Re}(p_\rho \mathbf{E}^{(\boldsymbol{\rho})}\cdot\mathbf{p} + p_\phi \mathbf{E}^{(\boldsymbol{\phi})}\cdot\mathbf{p} + p_z \mathbf{E}^{(\mathbf{z})}\cdot\mathbf{p}) \\ &= -\frac{1}{2}\mathrm{Re}[p_\rho(p_\rho E_\rho^{(\boldsymbol{\rho})} + p_\phi E_\phi^{(\boldsymbol{\rho})} + p_z E_z^{(\boldsymbol{\rho})}) + p_\phi(p_\rho E_\rho^{(\boldsymbol{\phi})} + p_\phi E_\phi^{(\boldsymbol{\phi})} + p_z E_z^{(\boldsymbol{\phi})}) + p_z(p_\rho E_\rho^{(\mathbf{z})} + p_\phi E_\phi^{(\mathbf{z})} + p_z E_z^{(\mathbf{z})})] \\ &= p_\rho^2\Gamma_{\mathrm{R}}^{(\boldsymbol{\rho})} + p_\phi^2\Gamma_{\mathrm{R}}^{(\boldsymbol{\phi})} + p_z^2\Gamma_{\mathrm{R}}^{(\mathbf{z})} - \frac{1}{2}\mathrm{Re}(p_\rho p_\phi E_\phi^{(\boldsymbol{\rho})} + p_\rho p_z E_z^{(\boldsymbol{\rho})} + p_\phi p_\rho E_\rho^{(\boldsymbol{\phi})} + p_\phi p_z E_z^{(\boldsymbol{\phi})} + p_z p_\rho E_\rho^{(\mathbf{z})} + p_z p_\phi E_\phi^{(\mathbf{z})}).\end{aligned} \tag{S12}$$

In Eq. (S12), the $\mathbf{r}_0$-dependence is omitted in all electric-field terms to simplify the symbols. Equation (S12) gives the relation between the total spontaneous emission rate $\Gamma_{\mathrm{T}}^{(\mathbf{p})}$ of a point source with an arbitrary linear-polarization direction and those $(\Gamma_{\mathrm{T}}^{(\boldsymbol{\rho})}, \Gamma_{\mathrm{T}}^{(\boldsymbol{\phi})}, \Gamma_{\mathrm{T}}^{(\mathbf{z})})$ of point sources polarized along the directions of three orthogonal basis vectors (**ρ**, **ϕ**, **z**). In the coupling system of a point source and a silver NW of infinite length, as shown in Fig. S9, there is $E_z^{(\boldsymbol{\rho})} = E_\phi^{(\boldsymbol{\rho})} = E_\rho^{(\boldsymbol{\phi})} = E_z^{(\boldsymbol{\phi})} = E_\rho^{(\mathbf{z})} = E_\phi^{(\mathbf{z})} = 0$ ($\mathbf{r}_0$-dependence is omitted) from the symmetry of the electromagnetic field. Then, Eq. (S12) reduces to

$$\Gamma_{\mathrm{T}}^{(\mathbf{p})} = p_\rho^2\Gamma_{\mathrm{T}}^{(\boldsymbol{\rho})} + p_\phi^2\Gamma_{\mathrm{T}}^{(\boldsymbol{\phi})} + p_z^2\Gamma_{\mathrm{T}}^{(\mathbf{z})}. \tag{S13}$$

From Eq. (S13), we can obtain

$$\min(\Gamma_{\mathrm{T}}^{(\boldsymbol{\rho})}, \Gamma_{\mathrm{T}}^{(\boldsymbol{\phi})}, \Gamma_{\mathrm{T}}^{(\mathbf{z})}) \le \Gamma_{\mathrm{T}}^{(\mathbf{p})} \le \max(\Gamma_{\mathrm{T}}^{(\boldsymbol{\rho})}, \Gamma_{\mathrm{T}}^{(\boldsymbol{\phi})}, \Gamma_{\mathrm{T}}^{(\mathbf{z})}), \tag{S14}$$

where $\min(\Gamma_{\mathrm{T}}^{(\boldsymbol{\rho})}, \Gamma_{\mathrm{T}}^{(\boldsymbol{\phi})}, \Gamma_{\mathrm{T}}^{(\mathbf{z})})$ and $\max(\Gamma_{\mathrm{T}}^{(\boldsymbol{\rho})}, \Gamma_{\mathrm{T}}^{(\boldsymbol{\phi})}, \Gamma_{\mathrm{T}}^{(\mathbf{z})})$ denote the minimum and maximum values of $(\Gamma_{\mathrm{T}}^{(\boldsymbol{\rho})}, \Gamma_{\mathrm{T}}^{(\boldsymbol{\phi})}, \Gamma_{\mathrm{T}}^{(\mathbf{z})})$, respectively.

F. Impact of the length and dimeter of silver nanowire on the fluorescence lifetime of molecules

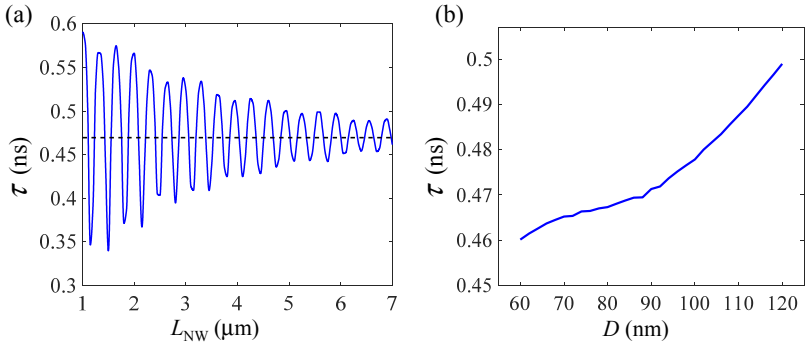

Fig. S10 Dependence of the fluorescence lifetime τ of A647 molecules on the length L_{NW} (**a**) and diameter D (**b**) of the silver NW based on Eq. (1) in the main text. In (a), D=90nm and the distances from the point source to both ends of the NW are equal. In (b), the length of the silver NW is infinite. The horizontal black-dashed line in (a) show the τ for a silver NW with an infinite length ($L_{\mathrm{NW}}\to\infty$). In (a) and (b), the point source is radially polarized, with a distance d=25nm to the surface of the NW. The results are obtained with the FEM.

As shown in Fig. S10(a), the fluorescence lifetime τ [given by Eq. (1) in the main text] of molecules oscillates quasi-periodically with the increase of length L_{NW} of the silver NW. This oscillation results from that the SPPs excited by the point source will be reflected when they arrive at the ends of the NW, and the reflected SPPs and the directly-excited SPPs will interfere constructively or destructively at the position of the point source, resulting in an increase or decrease of the total spontaneous emission rate Γ_{T}, and resultantly, a decrease or increase of τ. However, due to the propagation loss of SPPs, when the length L_{NW} of the NW exceeds 6μm, the reflected SPPs will be very weak when they propagate to the position of the point source, so that the fluctuation of τ caused by the increase of L_{NW} will be less than 0.035ns, and the value of τ will be close to that for $L_{\mathrm{NW}}\to\infty$ [shown by the horizontal black dashed line in Fig. S10(a)].

G. Expected value of the intensity $I_{\mathrm{SPP},p}$ of the SPP excited by a point source with a random linear-polarization direction

In this subsection, we consider the case that the linear-polarization direction of the point source is randomly oriented. In this case, the unit vector **p** along the polarization direction of the point source is regarded as a random variable, and consequently, the intensity $I_{\mathrm{SPP},p}$ of SPPs excited by the point source

becomes a random variable as well. We will present the calculation formula and results of the expected value $E(I_{\mathrm{SPP},p})$ of $I_{\mathrm{SPP},p}$. In the coupling system of a point source and a silver NW of infinite length, as shown in Fig. S9, $\mathbf{p}=\mathbf{p}(\theta,\varphi)=\boldsymbol{\rho}\sin\theta\cos\varphi+\boldsymbol{\phi}\sin\theta\sin\varphi+\mathbf{z}\cos\theta=p_\rho\boldsymbol{\rho}+p_\phi\boldsymbol{\phi}+p_z\mathbf{z}$, where θ and φ are random variables. Assuming that the probabilities of all orientations of $\mathbf{p}$ are equal, the joint probability density function of θ and φ should be

$$f(\theta,\varphi)=\begin{cases}\dfrac{1}{4\pi}\sin\theta, \text{ for } \theta\in[0,\pi],\ \varphi\in[0,2\pi],\\ 0, \text{ else.}\end{cases} \tag{S15}$$

According to the definition of SPP intensity $I_{\mathrm{SPP},p}$ in Section 3.2B of the main text, there is

$$I_{\mathrm{SPP},p}(\mathbf{r}_0)=\Gamma_{\mathrm{exc}}(\mathbf{r}_0)\eta_{\mathrm{SPP}}=\frac{1}{|\mathbf{E}_0|^2}|\mathbf{E}(\mathbf{r}_0)\cdot\mathbf{p}|^2\,\eta_{\mathrm{SPP}}(\mathbf{p}), \tag{S16}$$

where $\mathbf{E}(\mathbf{r}_0)$ is the electric-field vector at the position $\mathbf{r}_0$ of the point source excited by the illumination field, and $\mathbf{E}_0$ is the electric-field vector at the focal point excited by the illumination field in the absence of the silver NW. η_{SPP} is the coupling efficiency of SPP waveguide modes on the silver NW excited by the point source, and is defined as $\eta_{\mathrm{SPP}}=\Gamma_{\mathrm{SPP}}/\Gamma_\tau$, where $\Gamma_{\mathrm{SPP}}=\Gamma_{\mathrm{SPP1}}+\Gamma_{\mathrm{SPP2}}$ [see this before Eq. (2) in the main text]. $\eta_{\mathrm{SPP}}=\eta_{\mathrm{SPP}}(\mathbf{p})$ depends on $\mathbf{p}=\mathbf{p}(\theta,\varphi)$ and is a random variable as well. Note that the point source with a random linear-polarization direction $\mathbf{p}$ can excite both of the two degenerate SPP mode 2, that is, SPP mode (2, ρ, z) and mode (2, ϕ) [see their definitions before Eq. (2) in the main text]. There is $\Gamma_{\mathrm{SPP2}}=\Gamma_{\mathrm{SPP2},\rho,z}+\Gamma_{\mathrm{SPP2},\phi}$, where $\Gamma_{\mathrm{SPP2},\rho,z}$ is the coupling rate of SPP mode (2, ρ, z) excited by the $\boldsymbol{\rho}$- and $\mathbf{z}$-components (i.e., $p_\rho\boldsymbol{\rho}+p_z\mathbf{z}$) of the point source, and $\Gamma_{\mathrm{SPP2},\phi}$ is the coupling rate of SPP mode (2, ϕ) excited by the $\boldsymbol{\phi}$-component (i.e., $p_\phi\boldsymbol{\phi}$) of the point source. For the calculations of $\Gamma_{\mathrm{SPP2},\rho,z}$ and $\Gamma_{\mathrm{SPP2},\phi}$, one just needs to replace the $\mathbf{p}$ in Eq. (3) of the main text by $p_\rho\boldsymbol{\rho}+p_z\mathbf{z}$ and $p_\phi\boldsymbol{\phi}$, respectively. It should be noted that when $\mathbf{p}$ is replaced by $p_\rho\boldsymbol{\rho}+p_z\mathbf{z}$, $\Gamma^-_{\mathrm{SPP}i}=\Gamma^+_{\mathrm{SPP}i}$ no longer holds.

Using Eq. (S16), the expected value $E[I_{\mathrm{SPP},p}(\mathbf{r}_0)]$ of $I_{\mathrm{SPP},p}(\mathbf{r}_0)$ can be calculated as

$$E[I_{\mathrm{SPP},p}(\mathbf{r}_0)]=\int_0^\pi d\theta\int_0^{2\pi}d\varphi\frac{1}{|\mathbf{E}_0|^2}|\mathbf{E}(\mathbf{r}_0)\cdot\mathbf{p}(\theta,\varphi)|^2\,\eta_{\mathrm{SPP}}(\mathbf{p}(\theta,\varphi))f(\theta,\varphi). \tag{S17}$$

In addition, for a point source with a random linear-polarization direction, one can define

$$I^\pm_{\mathrm{SPP},p}(\mathbf{r}_0)=\Gamma_{\mathrm{exc}}(\mathbf{r}_0)\eta^\pm_{\mathrm{SPP}}, \tag{S18}$$

as the intensities of the forward (+) and backward (–) SPP waveguide modes propagating along the NW excited by the point source, where $\eta^\pm_{\mathrm{SPP}}=\Gamma^\pm_{\mathrm{SPP}}/\Gamma_\tau$ is the coupling efficiency, and $\Gamma^\pm_{\mathrm{SPP}}=\Gamma^\pm_{\mathrm{SPP1}}+\Gamma^\pm_{\mathrm{SPP2}}$ is the coupling rate of the forward and backward SPP waveguide modes. The expected value $E[I^\pm_{\mathrm{SPP},p}(\mathbf{r}_0)]$ of $I^\pm_{\mathrm{SPP},p}(\mathbf{r}_0)$ can be calculated simply by replacing η_{SPP} in Eq. (S17) by $\eta^\pm_{\mathrm{SPP}}$. Obviously, there is

$$I_{\mathrm{SPP},p}(\mathbf{r}_0)=I^+_{\mathrm{SPP},p}(\mathbf{r}_0)+I^-_{\mathrm{SPP},p}(\mathbf{r}_0),\quad E[I_{\mathrm{SPP},p}(\mathbf{r}_0)]=E[I^+_{\mathrm{SPP},p}(\mathbf{r}_0)]+E[I^-_{\mathrm{SPP},p}(\mathbf{r}_0)]. \tag{S19}$$

Figure S11(a) shows $E[I^+_{\mathrm{SPP},p}(\mathbf{r}_0)]$ and $E[I^-_{\mathrm{SPP},p}(\mathbf{r}_0)]$ plotted as functions of the molecule position $\mathbf{r}_0$. Here the $\mathbf{r}_0$ is on a cylindrical surface with a distance d=20 nm to the surface of the silver NW and above the PMMA-1 layer, as shown in Fig. 1(b) of the main text. The cylindrical surface corresponds to $\rho=R+d$, $z\in$(–400 nm, 400 nm) and $\phi\in(\phi_0,\ \pi-\phi_0)$ with $\phi_0=\arcsin[(h+d-R)/(R+d)]$ (R=45 nm, h=60 nm). The results indicate that, for a molecule with a random linear-polarization direction at any position in the excitation region, the expected values of the intensities of the excited forward and backward SPPs are equal, that is, $E[I^+_{\mathrm{SPP},p}(\mathbf{r}_0)]=E[I^-_{\mathrm{SPP},p}(\mathbf{r}_0)]$. Similarly, based on $\Gamma^-_{\mathrm{SPP}i}=\Gamma^+_{\mathrm{SPP}i}$ (i=1, 2), for molecules with radial, azimuthal and axial polarization directions, the intensities of the excited forward and backward SPPs are equal as well, that is, $I^+_{\mathrm{SPP},\rho/\phi/z}(\mathbf{r}_0)=I^-_{\mathrm{SPP},\rho/\phi/z}(\mathbf{r}_0)$, where the definition of $I^\pm_{\mathrm{SPP},\rho/\phi/z}(\mathbf{r}_0)$ is the same as that in Eq. (S18) with $\mathbf{p}$ being replaced by $\boldsymbol{\rho}$, $\boldsymbol{\phi}$ or $\mathbf{z}$, respectively. The distributions of $I^\pm_{\mathrm{SPP},\rho}(\mathbf{r}_0)$, $I^\pm_{\mathrm{SPP},z}(\mathbf{r}_0)$ and $I^\pm_{\mathrm{SPP},\phi}(\mathbf{r}_0)$ are shown in Fig. S11(b)-(d), respectively, which are plotted as functions of the molecule position $\mathbf{r}_0$.

Comparing Fig. S11(b) with (a), (c) and (d), it is evident that the intensity of SPPs excited by the radially polarized molecules is overall stronger than that by the randomly, axially or azimuthally polarized molecules. This further supports the explanation of the experimental results in Section 3.2B

of the main text: the SPPs whose scattered far field is collected from the remote ends of the silver NW are dominantly excited by the radially polarized molecules.

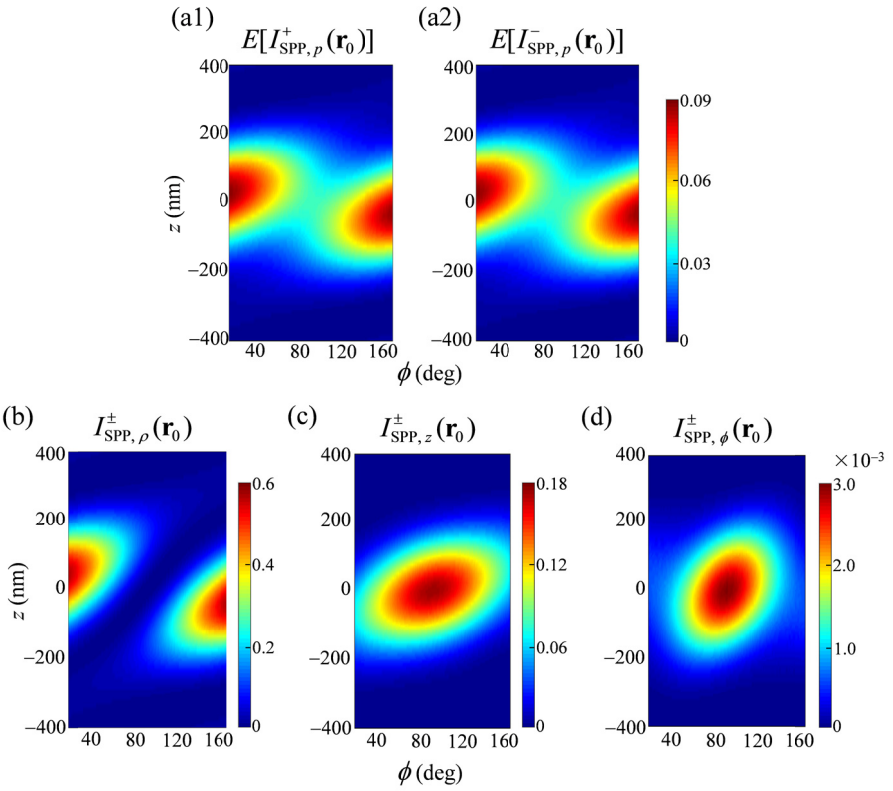

Fig. S11 Intensities of forward (+) and backward (–) SPPs excited by the molecules with a random (**a1**)-(**a2**), radial (**b**), axial (**c**) or azimuthal (**d**) polarization, which are plotted as functions of the molecule position $\mathbf{r}_0$ on a cylindrical surface with a distance d=20nm to the surface of the silver NW (radius R=45nm) and above the PMMA-1 layer [see Fig. 1(b) in the main text]. The cylindrical surface corresponds to $\rho=R+d$=65nm, $z\in$(–400nm, 400nm) and $\phi\in(\phi_0,\pi-\phi_0)$ (ϕ_0=arcsin[$(h+d-R)/(R+d)$], h=60nm). The molecules are excited by a tightly-focused (NA=1.49) circularly-polarized uniform plane wave with the focal point located at (ρ, ϕ, z)=(45nm, 90°, 0). The results are obtained with the FEM.

S3. Additional experimental and theoretical details for the remote axial localization of molecules

A. Derivation of Eq. (5) in the main text for the remote axial localization of a point emitter coupled with the silver nanowire

As shown in Fig. S12, the detection efficiencies of SPP mode i (i=1, 2) scattered at the left and right ends of the silver NW are defined as $\kappa_i^- = \Gamma_{i,\mathrm{collect}}^- / \Gamma_i^-$ and $\kappa_i^+ = \Gamma_{i,\mathrm{collect}}^+ / \Gamma_i^+$, respectively, where Γ_i^- and Γ_i^+ are the energy fluxes of SPP mode i excited by the point source when they arrive at the left and right ends of the NW, respectively. $\Gamma_{i,\mathrm{collect}}^-$ and $\Gamma_{i,\mathrm{collect}}^+$ are the energy fluxes of the scattered fields of SPP mode i collected by the objective lens from the left and right ends of the NW, respectively. It is assumed that the morphologies of the left and right ends of the NW are the same, i.e., $\kappa_i^- = \kappa_i^+ = \kappa_i$. On the cross-section (plane z=z_0 in Fig. S12) where SPPs begin to propagate, the initial energy fluxes $\Gamma_{\mathrm{SPP}i}^-$ and $\Gamma_{\mathrm{SPP}i}^+$ of left-going and right-going SPP mode i are abbreviated as Γ_{0i}^- and Γ_{0i}^+, respectively. It is assumed that $\Gamma_{\mathrm{SPP}i}^- = \Gamma_{\mathrm{SPP}i}^+$ [see the explanation after Eq. (5) in the main text], which then gives $\Gamma_{0i}^- = \Gamma_{0i}^+ = \Gamma_{\mathrm{SPP}i}/2$ with $\Gamma_{\mathrm{SPP}i} = \Gamma_{\mathrm{SPP}i}^+ + \Gamma_{\mathrm{SPP}i}^-$. According to the propagation law of SPP modes, there are

$$\Gamma_1^- = \Gamma_{01}^- \exp[-2k_0 L^- \mathrm{Im}(n_{\mathrm{eff}}^1)], \qquad \Gamma_1^+ = \Gamma_{01}^+ \exp[-2k_0 L^+ \mathrm{Im}(n_{\mathrm{eff}}^1)], \tag{S20a}$$

$$\Gamma_2^- = \Gamma_{02}^- \exp[-2k_0 L^- \mathrm{Im}(n_{\mathrm{eff}}^2)], \qquad \Gamma_2^+ = \Gamma_{02}^+ \exp[-2k_0 L^+ \mathrm{Im}(n_{\mathrm{eff}}^2)], \tag{S20b}$$

where $L^-=z_0-z^-$ and $L^+=z^+-z_0$ denote the axial distances from the point source to the left and right ends of the NW, $\mathrm{Im}(n_{\mathrm{eff}}^i)$ (i=1, 2) is the imaginary part of the complex effective index of SPP mode i, and $k_0=2\pi/\lambda$ is the wavenumber in the vacuum. The ratio of the energy fluxes of the SPPs' scattered fields collected from the left and right ends of the NW is

$$\frac{\Gamma_{\mathrm{collect}}^+}{\Gamma_{\mathrm{collect}}^-}=\frac{\Gamma_{1,\mathrm{collect}}^+ +\Gamma_{2,\mathrm{collect}}^+}{\Gamma_{1,\mathrm{collect}}^- +\Gamma_{2,\mathrm{collect}}^-}=\frac{\Gamma_1^+\kappa_1+\Gamma_2^+\kappa_2}{\Gamma_1^-\kappa_1+\Gamma_2^-\kappa_2}, \tag{S21}$$

where $\Gamma_{i,\mathrm{collect}}^{\pm}=\Gamma_i^{\pm}\kappa_i$ (i=1, 2) is used. For deriving Eq. (S21), it is assumed that the multiple reflection of SPPs at the two ends of the silver NW can be neglected, which holds for NWs that are long enough (for example, the NWs longer than 10 μm tested in the experiment, see Fig. S14). Substituting Eq. (20) into Eq. (21), we can obtain

$$\begin{aligned}\frac{\Gamma_{\mathrm{collect}}^+}{\Gamma_{\mathrm{collect}}^-}&=\frac{(\Gamma_{\mathrm{SPP1}}/2)\exp[-2k_0L^+\,\mathrm{Im}(n_{\mathrm{eff}}^1)]\kappa_1+(\Gamma_{\mathrm{SPP2}}/2)\exp[-2k_0L^+\,\mathrm{Im}(n_{\mathrm{eff}}^2)]\kappa_2}{(\Gamma_{\mathrm{SPP1}}/2)\exp[-2k_0L^-\,\mathrm{Im}(n_{\mathrm{eff}}^1)]\kappa_1+(\Gamma_{\mathrm{SPP2}}/2)\exp[-2k_0L^-\,\mathrm{Im}(n_{\mathrm{eff}}^2)]\kappa_2}\\&=\frac{\alpha\chi u_1u_3+u_2}{\alpha\chi u_3+1},\end{aligned} \tag{S22}$$

where $\alpha=\kappa_1/\kappa_2$, $\chi=\Gamma_{\mathrm{SPP1}}/\Gamma_{\mathrm{SPP2}}$, $u_1=\exp[-2\mathrm{Im}(n_{\mathrm{eff}}^1)k_0(z^-+z^+-2z_0)]$, $u_2=\exp[-2\mathrm{Im}(n_{\mathrm{eff}}^2)k_0(z^-+z^+-2z_0)]$, and $u_3=\exp[-2\mathrm{Im}(n_{\mathrm{eff}}^1-n_{\mathrm{eff}}^2)k_0(z_0-z^-)]$.

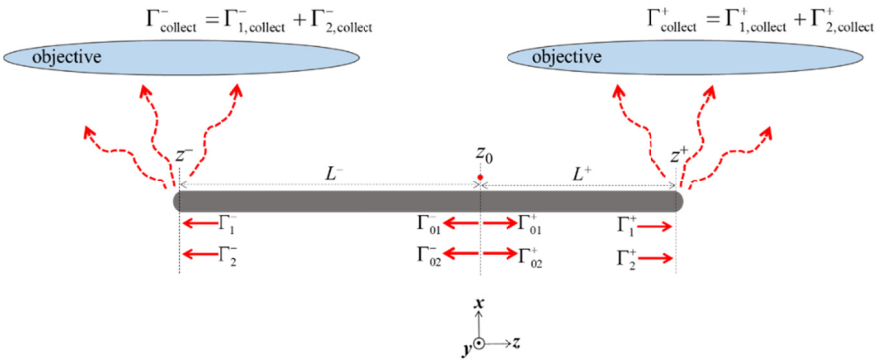

Fig. S12 Schematic diagram of the remote axial localization of an emitter coupled with the silver nanowire. The axial coordinate of the point source (represented by the red dot) is z_0, and the axial coordinates of the left and right ends of the silver NW are z^- and z^+, respectively. The initial energy fluxes of the backward and forward SPP mode i (i=1, 2) excited by the point source are Γ_{0i}^- and Γ_{0i}^+, respectively. The energy fluxes of the backward and forward SPP mode i are Γ_i^- and Γ_i^+ when they arrive at the left and right ends of the NW, respectively. The energy fluxes of the SPPs' scattered fields collected from the left and right ends of the NW by the objective lens are $\Gamma_{\mathrm{collect}}^-=\Gamma_{1,\mathrm{collect}}^-+\Gamma_{2,\mathrm{collect}}^-$ and $\Gamma_{\mathrm{collect}}^+=\Gamma_{1,\mathrm{collect}}^++\Gamma_{2,\mathrm{collect}}^+$, respectively, where $\Gamma_{i,\mathrm{collect}}^-$ and $\Gamma_{i,\mathrm{collect}}^+$ (i=1, 2) denote the energy fluxes of the scattered fields of SPP mode i collected from the left and right ends of the NW, respectively.

B. Values of the α and length of silver nanowires for the remote axial localization of molecules

For the ten silver NWs tested in Fig. 4(c) of the main text, the values of α in Eq. (5) obtained by a numerical fitting of the experimental data are shown in Fig. S13. The average value of the obtained α for the ten silver NWs is 12.4.

The central positions of the fluorescence spots at the two ends of the NW and the central position of the fluorescence spot in the excitation region are determined by a Gaussian fitting. The former are treated as the positions z^- and z^+ of the two ends of the NW, which then determine the length of the NW to be $L_{\mathrm{NW}}=z^+-z^-$, as shown in Fig. S14. The objective function of the Gaussian fitting is expressed as

$$\min_{\{I_0,\sigma_x,\sigma_y,x_0,y_0\}}\sum_m\sum_n\{\ln(I_{m,n})-\ln\{I_0\exp[-\frac{(x_m-x_0)^2}{2\sigma_x^2}-\frac{(y_n-y_0)^2}{2\sigma_y^2}]\}\}^2, \tag{S23}$$

where $I_{m,n}$ is the intensity distribution imaged by the EMCCD, which is the gray value of the mth-row

and nth-column pixel with a coordinate (x_m, y_n), and σ_x, σ_y, x_0, y_0 are the variables to be fitted, where (x_0, y_0) is the fitted central position of the fluorescence spot.

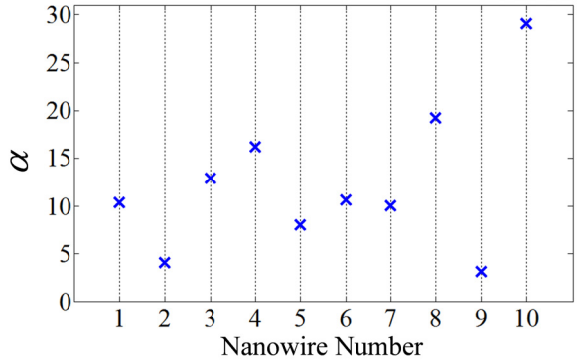

Fig. S13 For the ten silver NWs tested in Fig. 4(c) of the main text, the values of α obtained by numerical fitting (see Section 4 in the main text for the fitting method).

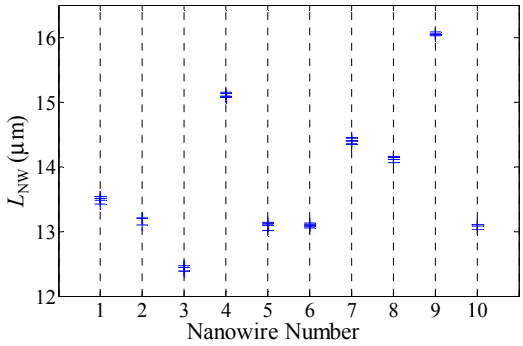

Fig. S14 Lengths L_{NW} of the ten silver NWs tested in Fig. 4(c) of the main text, which are obtained by a Gaussian fitting of the fluorescence spots at the two ends of the NW. The number on the horizontal axis represents the different NWs, and the different data points (represented by "+") for the same NW correspond to different fluorescence excitation positions.

References

1 J. P. Hugonin and P. Lalanne, *J. Opt. Soc. Am. A*, 2005, **22**, 1844-1849.

2 The calculation is performed with an in-house software: H. Liu, *DIF CODE for Modeling Light Diffraction in Nanostructures*, Nankai University, 2010.

3 T. Weiss, G. Granet, N. A. Gippius, S. G. Tikhodeev and H. Giessen, *Opt. Express*, 2009, **17**, 8051-8061.

4 D. Punj, M. Mivelle, S. B. Moparthi, T. S. van Zanten, H. Rigneault, N. F. van Hulst, M. F. Garcia-Parajo and J. Wenger, Nat. Nanotechnol., 2013, **8**, 512-516.